



# Impact of river water levels on the simulation of stream–aquifer exchanges over the Upper Rhine alluvial aquifer (France/Germany)

Jean-Pierre Vergnes<sup>1</sup> · Florence Habets<sup>2</sup>

Received: 12 September 2017 / Accepted: 25 April 2018 / Published online: 15 May 2018  
© The Author(s) 2018

## Abstract

This study aims to assess the sensitivity of river level estimations to the stream–aquifer exchanges within a hydrogeological model of the Upper Rhine alluvial aquifer (France/Germany), characterized as a large shallow aquifer with numerous hydro-power dams. Two specific points are addressed: errors associated with digital elevation models (DEMs) and errors associated with the estimation of river level. The fine-resolution raw Shuttle Radar Topographic Mission dataset is used to assess the impact of the DEM uncertainties. Specific corrections are used to overcome these uncertainties: a simple moving average is applied to the topography along the rivers and additional data are used along the Rhine River to account for the numerous dams. Then, the impact of the river-level temporal variations is assessed through two different methods based on observed rating curves and on the Manning formula. Results are evaluated against observation data from 37 river-level points located over the aquifer, 190 piezometers, and a spatial database of wetlands. DEM uncertainties affect the spatial variability of the stream–aquifer exchanges by inducing strong noise and unrealistic peaks. The corrected DEM reduces the biases between observations and simulations by 22 and 51% for the river levels and the river discharges, respectively. It also improves the agreement between simulated groundwater overflows and observed wetlands. Introducing river-level time variability increases the stream–aquifer exchange range and reduces the piezometric head variability. These results confirm the need to better assess river levels in regional hydrogeological modeling, especially for applications in which stream–aquifer exchanges are important.

**Keywords** Groundwater/surface-water relations · Numerical modeling · Transboundary aquifer · Wetlands · France · Germany

## Introduction

Regional alluvial aquifers are characterized by strong interactions between groundwater and surface water (Winter 1999; Woessner 2000; Sanford 2002; Sophocleous 2002; Thierion et al. 2012; Sun et al. 2016). Groundwater feeds rivers during dry periods, while rivers contribute to the recharge of aquifers under conditions of high water level that are associated with large precipitation or snowmelt. These stream–aquifer

exchanges make the alluvial hydrosystem vulnerable to pollution by anthropogenic sources. Upward capillary fluxes from shallow groundwater into the unsaturated soil column is also suspected to impact regional climate by modifying the water and energy exchanges between the ground surface and atmosphere, in particular by increasing evapotranspiration (Koster and Suarez 2001; Yeh and Eltahir 2005; Vergnes et al. 2014; Fan 2015; Döll et al. 2016). Therefore, the understanding of these interactions is essential for effective management of water resources as well as for estimating the impacts of anthropogenic activities or climate change.

Stream–aquifer exchanges are complex processes depending on climatic, hydrogeological, and geomorphological conditions (Winter 1999; Sophocleous 2002; Rupp et al. 2008). Their simulation usually requires the use of coupled surface-water/groundwater hydrological models. In general, a two-dimensional (2D) hydrogeological model is coupled to a hydrological model or a hydraulic model. Stream–aquifer exchanges can be represented either through a physically

---

✉ Jean-Pierre Vergnes  
jp.vergnes@brgm.fr

<sup>1</sup> BRGM French Geological Survey, Water Environment and Ecotechnologies Division, 3, avenue C. Guillemin, BP 36009, 45060 Orléans Cedex 2, France

<sup>2</sup> CNRS/Sorbonne University, UMR 7619 Métis, 4 place Jussieu, 75252 Paris cedex 5, France

based approach considering the hyporheic zone as a continuum interface, or by using a conductance model (Kollet and Maxwell 2006; Rushton 2007; Flipo et al. 2014). A conductance model computes the flux as the product between a transfer coefficient, depending on the riverbed characteristics, with the hydraulic head gradient between the river and the aquifer—for example, Sun et al. (2016) used the Soil and Water Assessment Tool (SWAT) semi-distributed model to study river water and groundwater exchange in an alluvial plain by using a new module based on conductance. In contrast, Kollet and Maxwell (2006) used an integrated surface-water/groundwater flow model that directly couples the governing equations of overland flow and variably saturated groundwater flow, thereby avoiding the need to define a transfer coefficient. The conductance model is commonly used at regional scale due to its good results with respect to the lower computational burden and the limited number of parameters involved, although the increase of computational capacity tends to make the physically based approach more feasible (Kollet and Maxwell 2006).

A lot of research has been carried out on the determination of the transfer coefficient (Rushton 2007; Fan et al. 2007). Indeed, this parameter represents control of the quantity of water that flows between the stream and the aquifer, and depends on several parameters such as the riverbed permeability or the temperature. Conversely, only a few studies have focused on the representation of the water level of rivers, yet it is a parameter of crucial importance in coupled models—for example, a spurious estimation of the river level may lead to surface-water bodies in the model that do not match their observed position and extent (Käser et al. 2014). Moreover, strong biases between observed and simulated piezometric heads or river water levels can also occur, particularly in alluvial plains where the water table is close to the surface. Even if the representation of river levels is taken into account in some hydrological models (Graham and Butts 2005; Doble et al. 2012, 2014; Zhang and Ross 2015; Thiéry 2015), its influence on the simulated stream–aquifer exchanges and groundwater flooding in regional hydrological modeling is still unclear.

The representation of river levels in coupled hydrogeologic-hydrologic models mainly depends on the way the topography and the river geometry are defined, and on the type of hydrological routing model that is used. In the case where the temporal variability of the river level is neglected, the river level is commonly derived from a digital elevation model (DEM). DEMs give access to the topography at regional scale using either airborne or remote-sensing techniques. In hydrological modeling, they are widely used to delineate watershed boundaries and stream networks. However, they are also associated with systematic errors related to the stream channel geometry (Orlandini and Rosso 1998; Paiva et al. 2011; Brasington et al. 2012; Käser et al. 2014), the presence of vegetation (Kellndorfer et al. 2004), surface-water effects (Schumann

et al. 2008) and random noise inherent to the measurement device (Rabus et al. 2003; Sun et al. 2003; Farr et al. 2007; Javernick et al. 2014). These errors typically result in unrealistic slopes along the drainage network and cause unrealistic “pits” (lows) and “dams” (high; Käser et al. 2014). The random noise can influence the simulated stream–aquifer exchanges; therefore, some methods have been proposed to deal with this problem—for example, Paiva et al. (2011) used a low-pass filter for removing the vegetation effect and random noise from the DEM. Moreover, DEMs do not always capture the fine-scale morphological features that are important for certain hydrological processes—for example, breaks-in-slope from weirs and dams of the stream surface are generally associated with the largest errors in DEMs, while they are major drivers of hyporheic exchanges (Heritage et al. 2009; Schächli et al. 2010; Käser et al. 2014). Lastly, a study conducted by Saleh et al. (2011) over the Oise River catchment in France showed that using fixed river levels in a coupled surface-subsurface hydrological model at a daily time step not only leads to biased assessments of stream–aquifer exchanges, but also to biased estimates of the near river piezometric head distributions.

Taking into account the temporal variability of river levels appears to be essential to improve both stream–aquifer exchanges and near-river piezometric heads. The fluctuations of river levels are commonly simulated either by using a variable velocity algorithm in a hydrological routing model (Saleh et al. 2011; Dai et al. 2015; Häfliger et al. 2015) or by using a hydrodynamic model based on the Saint-Venant equations (Thompson et al. 2004; Saleh et al. 2013; Barthel and Banzhaf 2016). Simulating variable river levels makes the representation of the river geometry essential for studying both flood inundation and stream–aquifer exchanges—for example, any deviation from a vertical representation of banks will increase the area of exchange during a stream flow event (Doble et al. 2012). However, the coarseness of the model resolution and the complexity of the stream channel morphology lead the modelers to use simplified hypotheses that raise new problems in representing these processes—for example, river geometry is often represented as a rectangular cross-section (Käser et al. 2014). In such cases, the unknown parameters refer to the width, the banks, and the bed of the river. At the regional scale, these parameters are often defined through simple geomorphological laws based on available observed datasets (Arora and Boer 1999; Decharme et al. 2008; Vergnes et al. 2014), which are not always appropriate to the geomorphological and climatic context. Moreover, the elevation of the riverbed is often derived from a DEM and therefore shares the associated uncertainties—as an example, Thierion et al. (2012) suggested that the use of spatially homogeneous riverbed parameters leads to smoother spatial variations of the simulated stream–aquifer exchanges along the river network compared to the observed ones.

In this context, the aim of this paper is to quantify how the representation of river levels affects the stream–aquifer exchanges and the groundwater floods in the context of an alluvial aquifer. This study focuses on the Upper Rhine Graben alluvial aquifer known for its strong stream–aquifer interactions (Trémolières et al. 1993) using the hydro(geo)logical modeling platform Eau-Dyssée. This model was first used by Thierion et al. (2012) on the Upper Rhine Graben using fixed river water levels and it is proposed here to use this modeling framework to compare different representations of the river levels in Eau-Dyssée.

## Methods

### The Upper Rhine Graben hydrosystem

A detailed description of the simulated domain can be found in Thierion et al. (2012). The main points are briefly recalled here. The Upper Rhine Graben is located in the eastern part of France along the border between France and Germany and extends from Basel in the south to Lauterbourg in the north as shown in Fig. 1. The red line delineates the contours of the whole modeled hydrosystem and the green line corresponds to the part where the aquifer is represented in the model. It is surrounded by the Vosges Mountain in the west and the Black Forest in the east and contains Quaternary gravels and sands which constitute the Rhine alluvial aquifer. This aquifer is characterized by high hydraulic properties with hydraulic

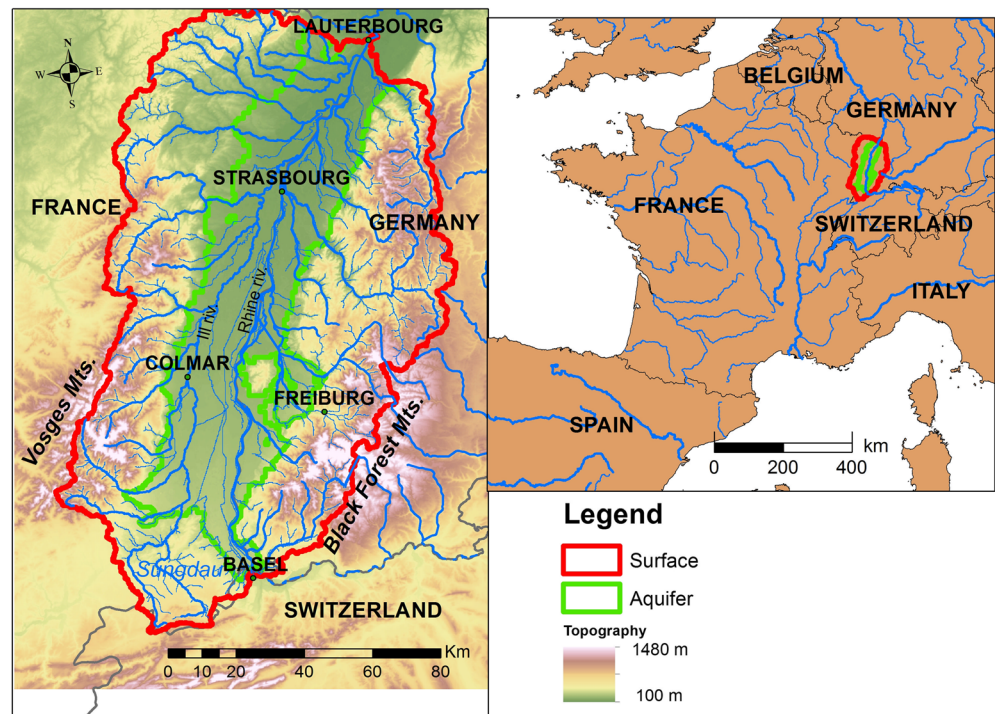
conductivity from  $10^{-4}$  to  $10^{-3}$  m/s (Majdalani and Ackerer 2011) and has a thickness that reaches more than 200 m at its center, east of Colmar, becoming shallow near the alluvial plain limits (LUBW 2006). Groundwater flows from south to north and is closer to the surface in the northern part of the aquifer. Water-table depths range from 0 to 20 m and groundwater wetlands are found in the middle and the northern parts of the plain.

The hydrographic network is very dense in the plain due to the presence of many groundwater-fed rivers, allowing significant exchange of water between the rivers and the aquifer. The main tributary of the Rhine in this part of the basin is the Ill River, which has its source in the Sundgau region of France (Thierion et al. 2012). Snow accumulation and melting are important processes for the dynamics of river flows in these catchments: snowfall accounts for around 3% of total precipitation in the plain and up to 37% at the mountaintops. As a consequence, the rivers flowing from the mountainous catchments play a crucial role in the recharge of the aquifer; moreover, the maximum flow of the Rhine River occurs at the end of spring due to the Alpine melting snow.

### The Eau-Dyssée hydrogeological modeling platform

The Eau-Dyssée modeling platform couples existing specialized models to address water resources and quality in regional-scale river basins (Saleh et al. 2013). The configuration used for the present application is composed of three modules corresponding to two hydrological components: the

**Fig. 1** Map of the case study area on a European map. Red lines correspond to the contours of the whole modeled domain and green lines correspond to the part where the aquifer is represented. The topography of the case study is shown in the background (m above sea level)



saturated zone or aquifer component based on the Simulation des Aquifères Multicouches (SAM) regional groundwater model (Ledoux et al. 1989), the in-stream water routing component based on the Routing Application for Parallel Computation of Discharge (RAPID) model (David et al. 2011), and the surface-water/groundwater interaction component, including river level fluctuations calculated by a module called QtoZ (Saleh et al. 2011).

The SAM model is a regional spatially distributed model that computes the temporal distribution of the piezometric heads of multilayer aquifer units using a square grid discretization, with a finite differences resolution of the diffusivity equation. In each aquifer, flows are bidimensionnal, whereas they are vertically monodimensionnal in the aquitard between two horizontal layers. The multilayer model simulates confined and unconfined aquifer units. The temporal variation of the hydraulic head is modeled by nonlinear Boussinesq. The former version of SAM has successfully predicted surface water and groundwater flow in many basins of varying scales and hydrogeological settings: the HAPEX-MOBILHY study (Boukerma 1987), the Rhône basin (Habets et al. 1999), the Seine basin (Gomez 2002), the Somme basin (Habets et al. 2010), the Loire basin (Monteil et al. 2010) and the Rhine basin (Thierion et al. 2012).

The RAPID model is a parallel computing-based river routing model based on the Muskingum routing scheme (David et al. 2011):

$$I-O = \frac{\Delta S}{\Delta t} \quad (1)$$

where  $I$  ( $\text{m}^3/\text{s}$ ) and  $O$  ( $\text{m}^3/\text{s}$ ) are the upstream and downstream discharges respectively, and  $\Delta S$  is the change in storage within the reach during a  $\Delta t$  time step. The storage  $S$  is related to both inflow and outflow:

$$S = k[\alpha I + (1-\alpha)O] \quad (2)$$

where  $k$  (s) is the transfer time between two adjacent river cells and  $\alpha$  is a weighting parameter. Further information on how these parameters are determined can be found in the section ‘The modeling setup’. RAPID is designed to be coupled with land surface models and groundwater models. It computes river flow and volume along a river network that was first discretized into square grid-cells. With such parametrization, the water is routed from upstream to downstream. The cells of this river network can be connected to the cells of the underlying groundwater models if an aquifer is present. In this case, the groundwater cells and the river cells have the same spatial resolution.

Surface-water/groundwater interactions are divided in two categories. First, the aquifer can be drained where the piezometric head reaches the soil level, which allows for simulating

groundwater overflow. Secondly, stream–aquifer exchanges are calculated in each river grid cell from the difference between hydraulic heads in the river cell and the underlying aquifer cell. Depending on the sign of this difference, surface water either infiltrates toward aquifer units, or groundwater exfiltrates toward surface water. The stream–aquifer exchanges  $Q_{\text{ex}}$  ( $\text{m}^3/\text{s}$ ) are computed as the product of a transfer coefficient  $T_p$  ( $\text{m}^2/\text{s}$ ), linked to the riverbed characteristics, by the difference between the piezometric head  $H_{\text{gw}}$  (m) and the elevation of the river level  $Z_{\text{riv}}$  (m):

$$Q_{\text{ex}} = \max(T_p(H_{\text{gw}} - Z_{\text{riv}}), Q_{\text{lim}}, Q_{\text{riv}}) \quad (3)$$

with  $Q_{\text{riv}}$  ( $\text{m}^3/\text{s}$ ) the available flow in the river cell that can be taken from the river before the river cell becomes dry. According to the sign convention within the model (fluxes are positive upward),  $Q_{\text{riv}}$  is negative since it corresponds to a flow from the river to the aquifer, while  $Q_{\text{ex}}$  is positive when water flows from the aquifer to the river, and negative otherwise.  $Q_{\text{lim}}$  ( $\text{m}^3/\text{s}$ ) is a maximum infiltration flow from the river to the aquifer, corresponding to the case when the piezometric head is below the riverbed (Rushton 2007) and is negative because it corresponds to a flow from the river to the aquifer. It depends on the area of the river cell. If this parameter is equal to zero, infiltration from stream to aquifer is not authorized even if the instream water level is higher than the water table.  $Q_{\text{lim}}$  can be estimated either from field measurements based on local mass balance or through available literature on riverbed permeability (Lange 2005). In this case, all the river cells have the same resolution and this parameter is constant and equal to  $-0.05 \text{ m}^3/\text{s}$ .

As the riverbed characteristics are mostly unknown, the coefficient  $T_p$  is often determined through calibration. Sensitivity analysis on this parameter can be found in Rushton (2007). Thierion et al. (2012) also performed a detailed sensitivity analyses on the  $T_p$  and  $Q_{\text{lim}}$  parameters for this case study: different values of  $Q_{\text{lim}}$  (0,  $-0.025$ ,  $-0.050$  and  $-0.1 \text{ m}^3/\text{s}$ ) were compared while keeping the  $T_p$  parameter equal to  $0.05 \text{ m}^2/\text{s}$ . In a similar way, different values of  $T_p$  (0.05, 0.1 and  $0.5 \text{ m}^2/\text{s}$ ) were compared using  $Q_{\text{lim}}$  equal to  $-0.05 \text{ m}^3/\text{s}$ . Results show that all these simulations could not be differentiated based regarding bias and root mean square error (RMSE) on the available wells except for two cases ( $Q_{\text{lim}} = 0 \text{ m}^3/\text{s}$  and  $Q_{\text{lim}} = -0.1 \text{ m}^3/\text{s}$ ) for which the water balance shows some differences. Finally, this study concluded that both infiltration and Rhine level variations are the most important processes in describing the interactions between the Rhine River and the aquifer, even though a finer calibration of  $T_p$  could be interesting to better represent the influence of the Rhine on the aquifer.

The module QtoZ allows one to calculate the river level for each river grid cell as a function of the discharge routed by RAPID (Saleh et al. 2011; Häfliger et al. 2015). The module

has three options for calculating river level in each river grid-cell: (1) fixed river level, (2) river level estimated from observed rating curves and (3) river level estimated from the inversion of the Manning Formula. For the two last options, observations can be used to derive the associated parameters locally, and a method has to be used to interpolate the value along the reach between two observations (Saleh et al. 2011; Häfliger et al. 2015). This step is not straightforward, and can lead to some errors that are sensitive when the module is coupled to groundwater modeling.

Within the Eau-Dyssée platform, the QtoZ module is coupled with the RAPID hydrological routing model and the SAM groundwater model. At each time step of the simulation, QtoZ receives discharge values from RAPID for each grid-cell and calculates a water level which is sent to SAM in order to simulate the river–aquifer exchanges for the next time step. This coupling is explicit since the river–aquifer exchanges used for the calculation of river discharges and piezometric heads are based on river levels calculated beforehand by QtoZ. Here, the river level impacts only the river–aquifer exchanges, although it could also affect the river flow velocity (Häfliger et al. 2015).

## The modeling setup

### Experiments

Eau-Dyssée is forced by recharge and surface runoff coming from the SURFace EXternalized (SURFEX) land surface model at a daily time step and over a 17-year period, starting from 1 July 1986 and ending on 31 July 2003 (Mahfouf et al. 1995; Noilhan et al. 2011; Masson et al. 2013). Four simulations were carried out and named according to their determination of river water levels, either with time-prescribed values (P) or time-variable values (V):

- PSRTM uses the Shuttle Radar Topography Mission (SRTM) topographic dataset to define prescribed river levels.
- PHY uses prescribed hydrological water levels coming both from a refined topography and from a hydraulic model for the Rhine River in order to account for the effect of the numerous dams.
- VMAN uses variable river water levels defined through a first method based on the Manning formula.
- VRC uses variable river water levels defined through a second method based on rating curves computed with both observed river levels and river discharges.

The specific topography used for the PHY simulation is defined using a simple moving average applied to the topography profile along the river network (that is, only along the river cells) in order to suppress the errors inherent to the

SRTM DEM. The window size of the moving average is equal to 1.8 km. This value was chosen in order to be sufficiently large to suppress the topography noise while keeping the first-order variation of topography. Moreover, simulated mean river levels coming from a fine-tuned hydrodynamic model covering the 1986–2003 period were chosen over the Rhine River in order to account for the numerous dams. This hydrodynamic model was built in the framework of a European research project on the modeling of nitrate pollution in the Upper Rhine Graben aquifer (LUBW 2006). It was built in order to finely represent the river-water-level variations of the Rhine River by taking into account all the available information on the geometry and the hydraulic characteristics of the river, including the influence of the dams (more details can be found in LUBW 2006).

For VMAN, Manning's formula converts the river discharge simulated by RAPID into a river level. With the hypothesis of a rectangular cross-section of the river, the hydraulic radius from Manning's formula is approximately equal to the river stage. Considering that the river bankfull height is smaller compared to the width of the river, Manning's formula can be rewritten as follows:

$$Z_{\text{riv}} = Z_{\text{bottom}} + H_{\text{riv}} \quad (4)$$

$$H_{\text{riv}} = \left[ \frac{Q_{\text{riv}} n}{W s^{0.5}} \right]^{\frac{3}{5}} \quad (5)$$

where  $Z_{\text{riv}}$  is the elevation of the river level,  $Z_{\text{bottom}}$  the elevation of the riverbed,  $H_{\text{riv}}$  the river level,  $Q_{\text{riv}}$  the simulated river discharge,  $n$  the Manning coefficient,  $W$  (m) the river width and  $s$  (m/m) the river slope.  $n$  is uniform and is equal to 0.04 over each river cell. One issue is to define  $W$  and  $Z_{\text{bottom}}$  for each river cell. To do so,  $W$  is defined using a specific geomorphological relationship that was established based on observations:

$$W = 5.41 \overline{Q_{\text{riv\_obs}}}^{0.55} \quad (6)$$

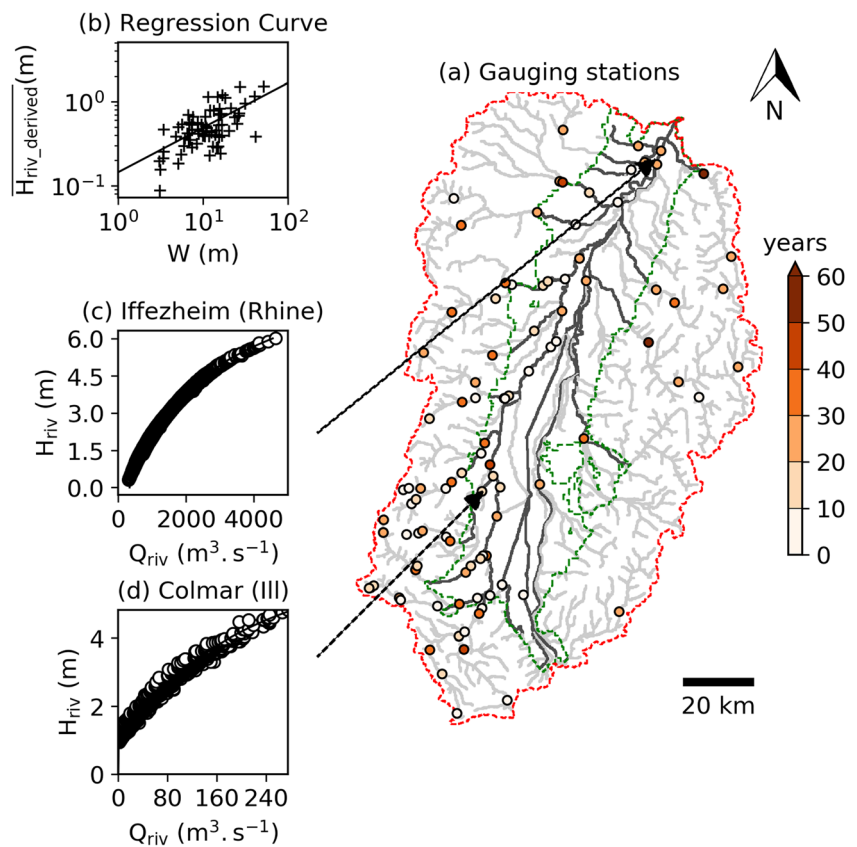
where  $\overline{Q_{\text{riv\_obs}}}$  corresponds to the mean observed river discharge on the full available period.  $Z_{\text{bottom}}$  was then defined as the difference between the prescribed elevation of river levels  $H_{\text{riv\_PHY}}$  (m) used for PHY and a specific mean river depth  $\overline{H_{\text{riv\_derived}}}$  (m) is defined as follows:

$$Z_{\text{bottom}} = H_{\text{riv\_PHY}} - \overline{H_{\text{riv\_derived}}} \quad (7)$$

$$\overline{H_{\text{riv\_derived}}} = 0.14 W^{0.53} \quad (8)$$

Equations (6) and (8) were derived as follows: observed mean river discharges and mean river water depths were calculated from 101 gauging stations distributed over the simulated domain (see Fig. 2). Equation (8) was derived using a least square regression with a correlation coefficient equal to

**Fig. 2** **a** Spatial distribution of the 101 selected gauging stations with their measurement times (years). The red-dashed line delineates the limits of the whole modeled hydrosystem and the green-dashed line corresponds to the part where the aquifer is represented in the model. River grid cells in dark gray correspond to the meshes where a rating curve is defined. **b** Regression curve between  $\overline{H}_{riv\_derived}$  and  $W$ . Example of rating curves computed for **c** the Rhine and **d** the Ill rivers are also shown. Circles correspond to the observations and solid lines correspond to the regression curves between  $H_{riv}$  and  $Q_{riv}$



–0.95. More details about these gauging stations can be found in the next section. River widths were determined from the “Système Relationnel d’Audit de l’Hydromorphologie des Cours d’Eau” (SYRAH) database (Chandesris et al. 2009) at each river gauging station. Figure 2a gives the spatial distribution of these gauging stations and the duration of their measurements. Figure 2b shows the regression curve obtained by plotting the river widths  $W$ , computed with Eq. (6), versus the observed mean river water depths. This regression corresponds to Eq. (8).  $W$  is estimated for each river grid cell using the mean simulated annual discharges computed from the total runoff, which corresponds to the sum of the recharge and the surface runoff, coming from SURFEX. River widths computed along the Rhine River spanned from 250 to 270 m. Despite this method not taking into account dams or weirs, it allows computation of the river widths for each grid cell of the river network, with no observations and with good order of magnitude. It is inspired by a similar method that was used in a previous study conducted in France by Vergnes et al. (2014) with a better accuracy provided by the use of the observations in the basin. Lastly, the riverbed slope  $s$  was computed using  $Z_{bottom}$ .

For the VRC simulation, a strategy is proposed to benefit from the 37 observed river levels and discharges available over the simulated aquifer domain delimited by green-dashed lines in Fig. 2a. First, functional relationships between

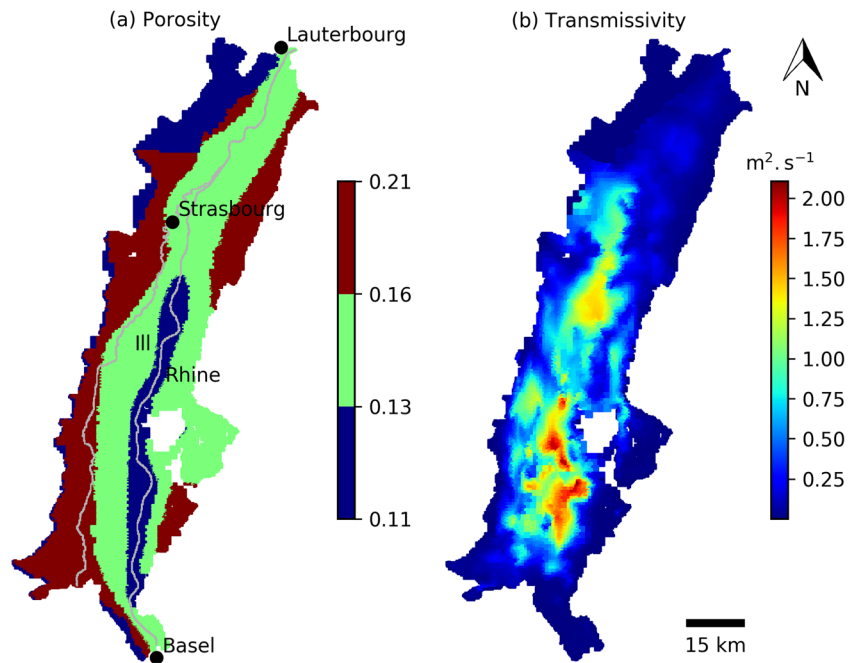
river levels and discharges (rating curve) are derived for each of these observations. Two examples of these rating curves are shown for the Rhine River at Iffezheim (Fig. 2b) and the Ill River at Colmar (Fig. 2c). River levels used for these rating curves correspond to the  $H_{riv}$  term of Eq. (4). The elevation of the river level  $Z_{riv}$  is then calculated using Eq. (4) with the same  $Z_{bottom}$  already used for VMAN. Last, each river grid-cell is attributed the rating-curve corresponding to the nearest gauging station along the river. Rating curves are attributed to river grid-cells only if the river is monitored by gauging stations. These rivers are represented by black lines in Fig. 2a. If no gauging stations are available, a constant river level is used as for the PHY simulation. The river grid-cell rating curves are input data for the QtoZ module.

Whatever the method used, the QtoZ module provides a water level to the SAM groundwater model as a function of the discharge routed by RAPID. Finally, SAM uses water levels to simulate and quantify the exchanges between the stream grid-cells and the aquifer grid-cells.

### Hydrodynamic parameters and boundary conditions

A detailed description of the modeling framework of the Rhine Upper Graben hydrosystem is given in Thierion et al. (2012) and is only summarized here. Figure 3 shows the spatial distribution of transmissivity and porosity (the storage

**Fig. 3** Spatial distribution of **a** porosity and **b** transmissivity over the Upper Rhine alluvial aquifer. The main cities and the Ill and Rhine rivers are also shown



coefficient used in the model being considered to be the aquifer porosity divided by the thickness of the aquifer) over the whole alluvial aquifer. Transmissivities correspond to the values derived by Majdalani and Ackerer (2011), while porosities correspond to the values that were calibrated in LUBW (2006) for the modeling of nitrate pollution in the Rhine Upper Graben aquifer. Two different boundary conditions were imposed. First, the temporal variation of the Rhine River discharge is imposed at Basel in the south. Secondly, a constant piezometric head is imposed at the northern and southern boundaries. The basin is discretized with square cells ranging in size from 200 m for the river cells to 1,600 m. The alluvial aquifer was represented by a single layer. There are a total of 34,180 aquifer cells and 26,013 river cells.

Subsurface flow at the western and eastern borders of the aquifer is known to be a significant part of the recharge. It was represented by specific boundary conditions in the model: the surface runoff reaching the aquifer surface on the bordering cells infiltrated to the water table and thus contributed to the aquifer recharge. This process is called lateral subsurface flow hereafter. The transfer coefficient for the stream–aquifer exchanges,  $T_p$ , is taken as uniform and equal to  $0.05 \text{ m}^2/\text{s}$ , while the maximum infiltration flow  $Q_{\text{lim}} = -0.05 \text{ m}^3/\text{s}$  for a 200-m square cell. These values correspond to the best estimates obtained through the sensitivity studies carried out by Thierion et al. (2012).

Regarding river routing, the  $k$  transfer time of RAPID (Eq. 2) was determined using a relative transfer time that is computed for each river cell based on topography and concentration time (Ledoux et al. 1984; Saleh et al. 2011). The transfer time  $k$  used in RAPID for the Upper Rhine Graben hydrosystem varies from 100 to 1,000 s for a

spatial discretization of 200 m, which is consistent for such a river network, and  $\alpha$  is equal to 1 since all the river cells have the same size.

#### Evaluation dataset

Piezometric level data came from 190 observation wells sampled weekly, only a few of them giving daily data. These observation wells are managed mainly by the APRONA (Association pour la PROtection de la Nappe d’Alsace) on the French side and by the LUBW-Baden-Württemberg (Landesanstalt für Umwelt, Messungen und Naturschutz in Baden-Württemberg) on the German side (Thierion et al. 2012).

Observed mean river discharges and maximum river levels were selected from 101 gauging stations available over the Upper Rhine Graben hydrosystem. The locations of these 101 gauging stations are shown in Fig. 2a. All these stations are inside the modeled hydrosystem represented by the red-dashed lines in Fig. 2a—86 are located in the French part of the domain and 15 in the German part of the domain. Data on the French side were obtained from the HYDRO database (Ministère de l’Ecologie, du Développement Durable et de l’Energie 2015) and data on the German side were obtained from the LUBW-Baden-Württemberg. They were used to compute the geomorphological relationships described by Eqs. (6) and (8). From these 101 gauging stations, 37 are located inside the aquifer domain limited by the green dashed lines.

Observed wetlands in the alluvial plain were extracted from the RAMSAR Sites Information Service (The Ramsar Convention Secretariat 2014) which provides online

information on wetlands that have been designated as internationally important (RAMSAR Sites) under the Convention on Wetlands. Supplementary data coming from the Natura 2000 network have also been used to complete these datasets.

### Results

All the results shown in this section refer to the whole period of simulation that spans from 1 July 1986 to 31 July 2003. Figures 4 and 5 show the spatial distribution of the biases and the RMSE respectively between the observed and simulated piezometric heads for the four simulations at each of the 190 piezometers. In all, 60% of the PHY piezometric heads range between  $-1$  and  $1$  m in terms of bias, while 84% have a RMSE score below  $1$  m (Fig. 4). This percentage decreases to 38.4 and 74% respectively with the PSRTM simulation. This

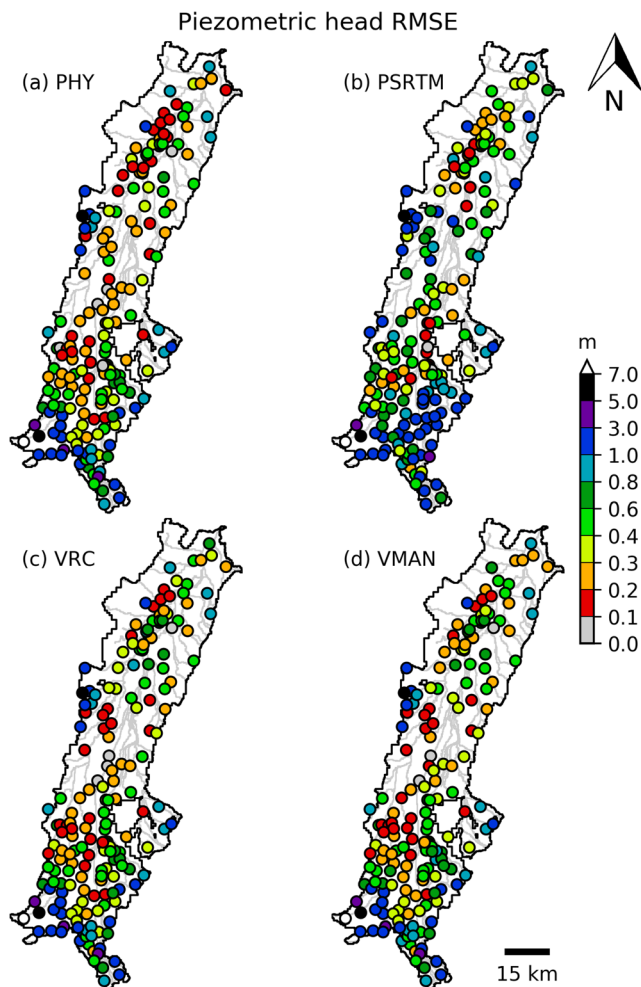


**Fig. 4** Spatial distributions of the RMSE between the observed and simulated piezometric heads at the 190 observation wells over the 1986–2003 period for the **a** PHY, **b** PSRTM, **c** VRC and **d** VMAN simulations

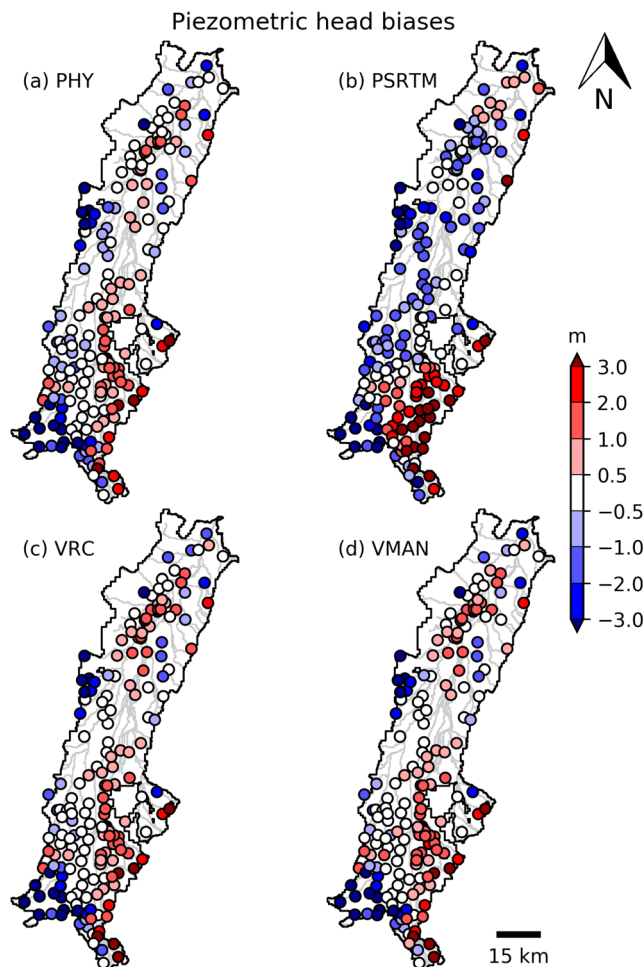


**Fig. 5** Spatial distributions of the biases between the observed and simulated piezometric heads at the 190 observation wells over the 1986–2003 period for the **a** PHY, **b** PSRTM, **c** VRC and **d** VMAN simulations

difference is due both to the underestimation of the piezometric heads located in the eastern border of the aquifer and to the overestimation in the south-eastern part of the domain. VMAN and VRC exhibit about 55 and 54% of piezometric heads ranging between  $-1$  and  $1$  m in terms of bias respectively. These percentages are slightly deteriorated compared to PHY, due to a more pronounced positive bias occurring along the Rhine River when using fluctuating river levels. However, about 84% of the simulated piezometric heads have a RMSE score below  $1$  m with both VMAN and VRC, which is the same percentage as for the PHY prescribed-values simulation (Fig. 5), which can be explained by the gain obtained with the river fluctuating levels in terms of amplitudes that compensate the more pronounced mean biases. At least, negative and positive biases are present in the south-western and south-eastern part of the aquifer respectively for all the simulations, especially for PSRTM (Fig. 4). These positive biases can be attributed to the uncertainties inherent to the SRTM topographic data as discussed later.



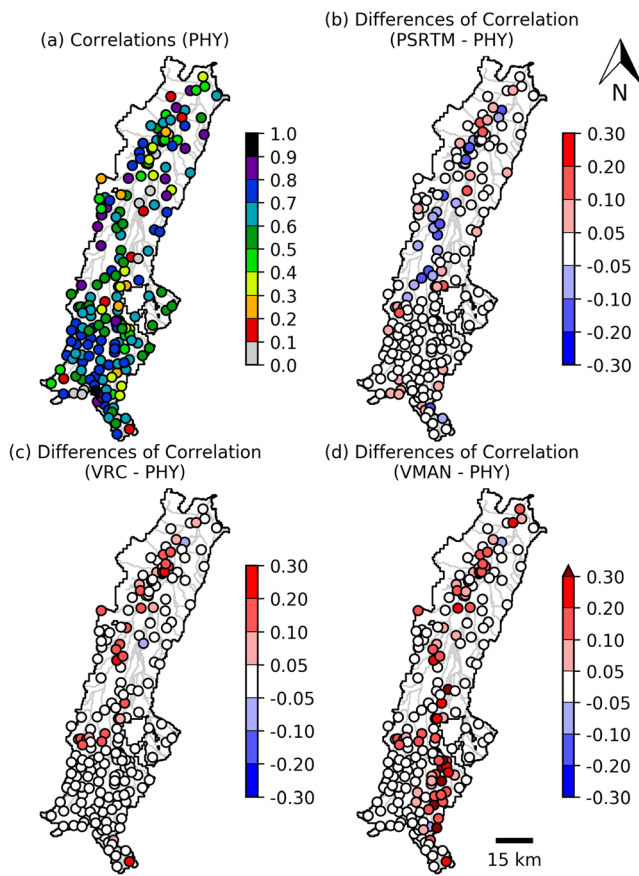


**Fig. 6** Comparison in terms of correlation between the observed and simulated piezometric heads at the 190 observation wells over the 1986–2003 period for the PHY, PSRTM, VRC and VMAN simulations. **a** The correlation coefficients for PHY are given together with the differences of correlation between **b** PSRTM and PHY, **c** VRC and PHY, and **d** VMAN and PHY. The calculated correlation corresponds to the covariance of the simulation and the observation divided by the product of their standard deviations

Figure 6 compares the observed and simulated piezometric heads in terms of correlation at each of the 190 selected piezometers. The correlation coefficient corresponds here to the covariance of the simulated and observed piezometric heads divided by the product of their standard deviation. The PHY simulation is given as the reference simulation. Each simulation is then compared to PHY in terms of correlation differences. No significant pattern can be found for PHY, except that the scores are slightly deteriorated near the Rhine River. The PRSTM simulation generally gives poorer results than PHY; however, the VRC and VMAN simulations improve the scores, especially along the Rhine River. In particular, the VMAN simulation gives better correlations in the southern part along the Rhine River; thus, 17% of the scores are improved with VRC and 35% with VMAN.

In Fig. 7, the spatial impact of the river level fluctuations on the distribution of piezometric heads is characterized at each aquifer cell by calculating the temporal

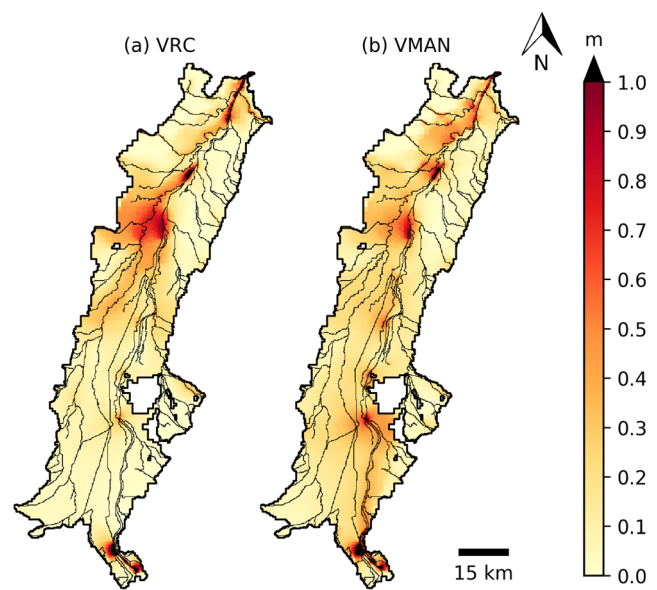


**Fig. 7** Mean absolute differences (MAD) computed for **a** VRC and **b** VMAN with respect to PHY

mean absolute differences (MAD) between the piezometric heads with and without taking into account water level fluctuations:

$$MAD = \frac{1}{N} \sum_{i=1}^N |H_{fix}(t_i) - H_{var}(t_i)| \tag{9}$$

where  $H_{fix}(t_i)$  (m) is the simulated piezometric head at a given time using a constant river water level corresponding to the PHY simulation,  $H_{var}(t_i)$  (m) is the simulated piezometric head using variable river levels and  $N$  is the number of time steps.

The spatial distribution of MAD varies from a few centimeters to more than 1 m. A strong pattern appears at the main confluences between the Rhine River and its tributaries, while the main impact is located along the Rhine River; moreover, the impact of the fluctuating river levels with VMAN concerns a wider area than with VRC.

Figure 8 shows the spatial distribution of biases between the observed and simulated river levels for all the simulations at each of the 37 available gauging stations. In all, 62% (11%) of the PHY (PSRTM) biases range between  $-1$  and  $1$  m and 19% (60%) are greater than  $1$  m, which shows that PSRTM strongly overestimates the river levels, whereas 41% (51%) of the VRC (VMAN) biases range between  $-1$  and  $1$  m, which shows that VMAN better reproduces the mean river levels than VRC. The VRC and VMAN simulations tend to overestimate river levels in the northern part of the aquifer. As previously shown in Fig. 6 for the piezometric heads, Fig. 9 shows the correlation coefficient for PHY and the differences of correlation between PSRTM and PHY, VRC and PHY, and VMAN and PHY. The median correlation coefficients are

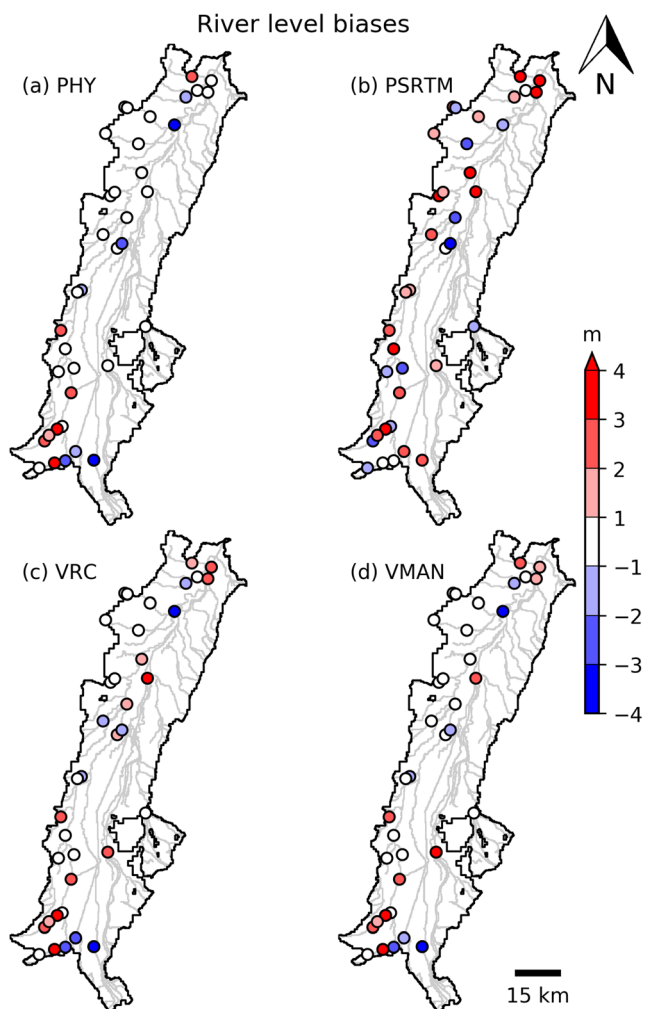


**Fig. 8** Spatial distribution of the biases between the simulated and observed river levels for **a** PHY, **b** PSRTM, **c** VRC and **d** VMAN

equal to 0.63, 0.62, 0.66 and 0.68 for PHY, PSRTM, VRC and VMAN respectively. Altogether, 80% of the simulated piezometers have a correlation coefficient greater than 0.42 for PHY, 0.43 for PSRTM, 0.46 for VRC and 0.51 for VMAN. The correlations given in Fig. 9 show that VMAN reproduces the river levels slightly better than VRC. These results agree with the previous comparison of piezometric heads (see Fig. 5); however, they should be treated with caution considering the small number of river level measurements compared to the number of piezometers.

Figure 10a,b focuses on the Ill and the Rhine rivers, respectively, by giving the profiles of the annual mean river levels and the stream–aquifer exchanges estimated by each simulation. Table 1 gives the repartition of the stream–aquifer exchanges between the positive (infiltration toward the aquifer) and negative (aquifer feeding the river) fluxes for both rivers and for each simulation. The PSRTM river level is unrealistic and noisy and hence gives strong variations of the stream surface for both the rivers. These errors lead in turn to noisy stream–aquifer exchanges characterized by strong and

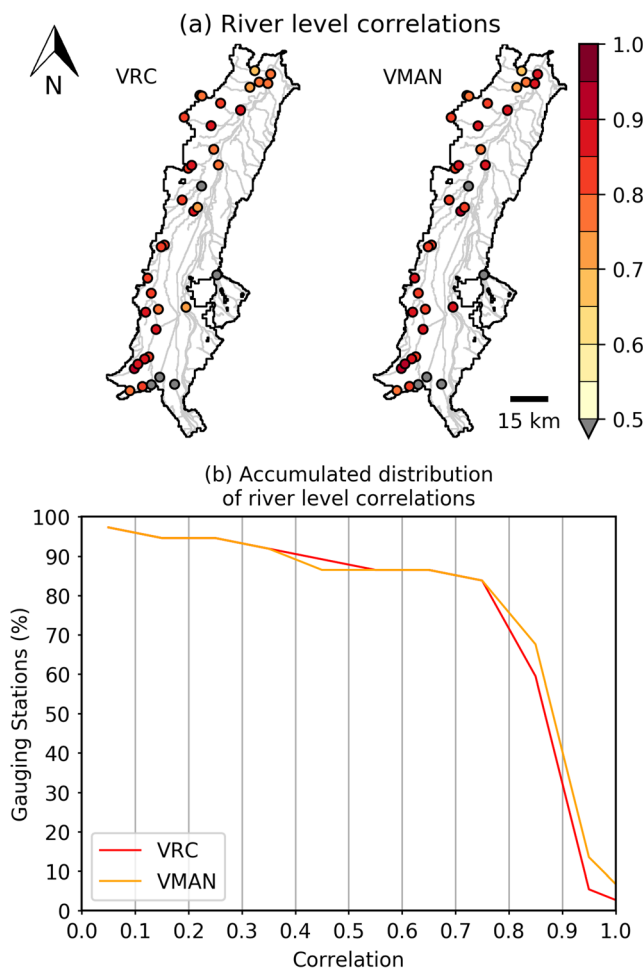


**Fig. 9** **a** Spatial distribution of river level correlations for VRC and VMAN. **b** The accumulated distribution of river level correlations, shown for VRC and VMAN. The y-axis corresponds to the percentage of the 37 available gauging stations for which the correlation is greater than the corresponding correlation on the x-axis

unrealistic peaks in the signal. The profiles of the other simulations are smoother due to the moving average filter with a 1.8-km window size applied to the elevation of the river surface. For the Ill River, the profile of the VRC river level is generally higher than VMAN and results in a decrease of the recharge to the aquifer; thus, the VRC stream–aquifer exchange curve is lower than the VMAN curve in Fig. 10a. Upstream, the river exclusively feeds the aquifer (negative flux), while closer to the outlet, the river mostly feeds the aquifer. For the Rhine River, the profiles of the river levels simulated with PHY, VRC and VMAN reflect the channelized shape of the river and its numerous dams. As a consequence, the stream–aquifer exchanges are negative all along the Rhine River, except sometimes in the neighborhood of the dams.

Figure 11 gives the spatial distribution of the mean water-table depths as well as the delineation of the observed wetlands from the RAMSAR and Natura 2000 datasets. The red color corresponds to the simulated groundwater overflow, that is, where the simulated piezometric head is equal to or above

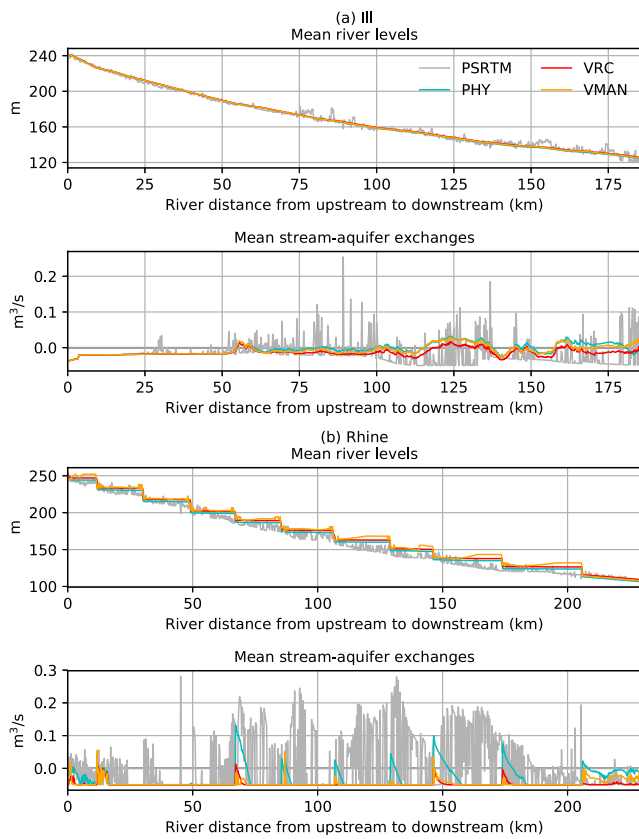


**Fig. 10** Annual mean river levels and annual mean stream–aquifer exchanges along **a** the Ill River and **b** the Rhine River

the topography. A visual overview reveals that the observed and simulated groundwater overflow agree relatively well for all the simulations except for PSRTM. This is especially the case along the Rhine River. Groundwater flooding is overestimated over the western part of the alluvial plain. To complete these results, the accumulated distribution of the mean water-table depths located over the observed wetlands are plotted in Fig. 12 for each simulation. Wetlands in this area are expected to correspond to areas where groundwater overflows;

**Table 1** Repartition in percentage of the total recharge between river-to-aquifer and aquifer-to-river exchanges over the 1986–2003 period along the Ill River and the Rhine River

River	Simulation	River to aquifer	Aquifer to river
Ill	PHY	65.6	34.4
	PRSTM	81.5	18.5
	VRC	86.9	13.1
	VMAN	71.9	28.1
Rhine	PHY	89.7	10.3
	PSRTM	64.7	35.3
	VRC	99.4	0.6
	VMAN	99.4	0.6

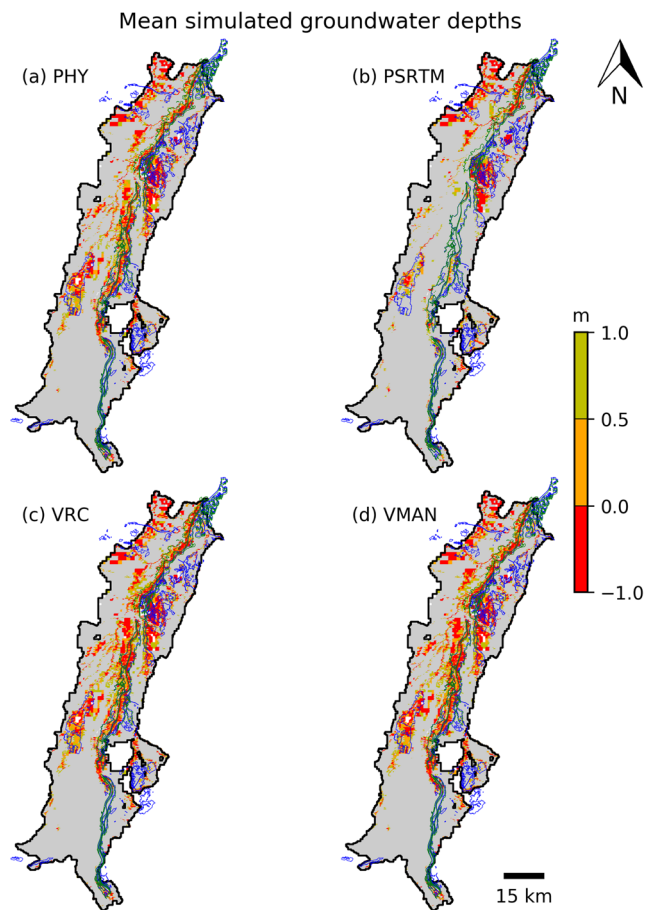


**Fig. 11** Spatial distribution of the simulated mean water-table depths for **a** PSRTM, **b** PHY, **c** VRC and **d** VMAN. Negative depths (red color) correspond to groundwater flooding. The RAMSAR and Natura 2000 datasets are delineated in green and blue respectively

that is, negative values in Fig. 12. The more the curve is shifted toward the right, the more the simulation agrees with the observed wetlands. The PHY, VMAN and VRC simulations outperform the PSRTM simulation. These results show the

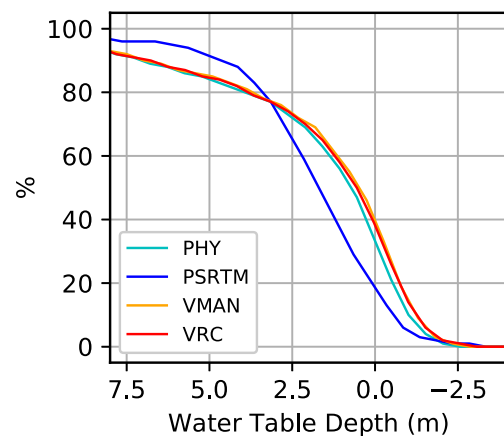
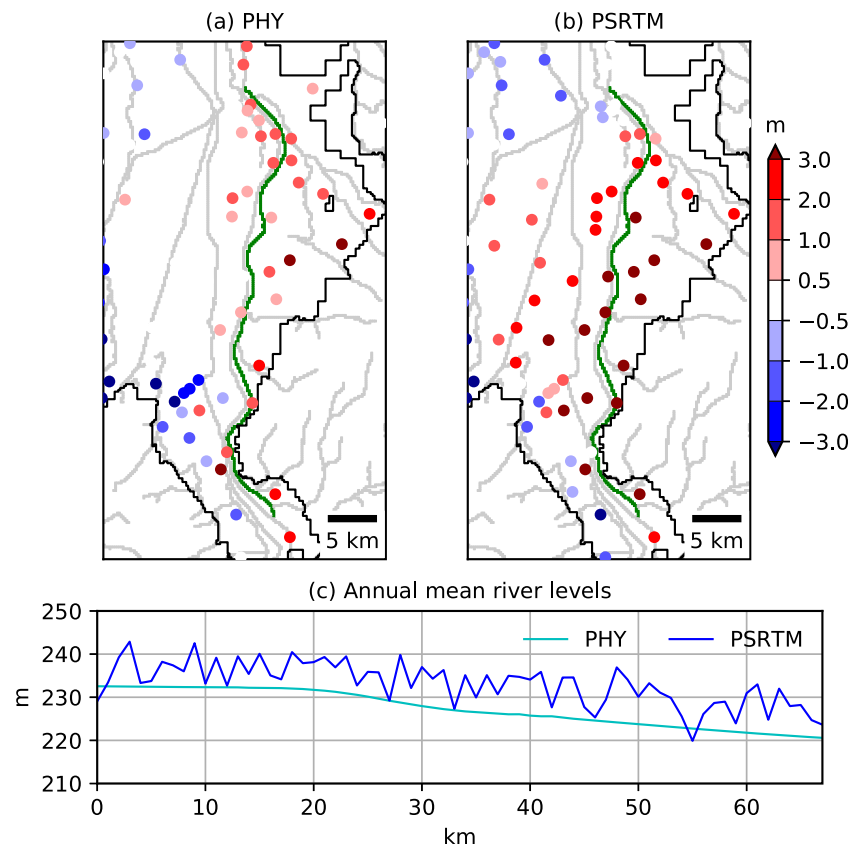


**Fig. 12** Accumulated distribution of the mean water-table depths located over the observed wetlands in Fig. 11 for the PHY, PSRTM, VMAN and VRC simulations

**Fig. 13** Spatial distribution of piezometric biases for **a** PHY and **b** PSRTM near the first tributary of the Rhine (in green). **c** The profiles of the annual mean simulated river levels



importance of representing a more realistic topography when simulating groundwater flooding. The VMAN and VRC simulations give slightly better results than the PHY simulation.

## Discussion and conclusions

The results presented in this study confirm the importance of a good representation of the river water level in a context of alluvial plains (Käser et al. 2014). Two kinds of improvement were shown to be useful: (1) a finer description of the river topography, and (2) a temporal variation of the river water level. Indeed, a spurious estimation of the river level leads to strong biases in the simulation of the piezometric heads and unrealistic stream–aquifer exchanges. Such spurious estimations are linked to the error regarding specifying the elevation of the river level or its riverbed, due to the noise inherent in the satellite-based DEM used for defining the channel topography (Sun et al. 2003; Kelldorfer et al. 2004; Schumann et al. 2008; Paiva et al. 2011; Käser et al. 2014). In the case of a conductance model, which is commonly employed in regional hydrogeological models, these noises strongly affect the sign of the hydraulic head gradient between the river and the aquifer. In this case, this leads to strong unrealistic negative (the rivers feeds the aquifer) or positive (the aquifer feeds the rivers) peaks, as shown in Fig. 10. Since the stream–aquifer

exchanges represent about 80% of the total recharge over the Upper Rhine aquifer (Thierion et al. 2012), these topographic errors can be the source of strong biases when simulating groundwater.

In order to avoid these errors, two corrections were applied. First, a low-pass filter was applied in order to obtain a continuous downstream slope along the drainage network (Paiva et al. 2011; Käser et al. 2014). This helps to suppress the unrealistic peaks of stream–aquifer exchanges and, in turn, to reduce the biases between the observed and simulated piezometric heads. Secondly, a fine-tuned river level was chosen along the Rhine River. This new river level takes into account the numerous dams built along the Rhine River and therefore allows one to simulate more realistic stream–aquifer exchanges. Indeed, the Rhine River has been strongly channelized in order to avoid groundwater flood inundation. As a consequence, the infiltration through the bottom of the Rhine riverbed became the main process for feeding the groundwater stream (Trémoilières et al. 1993). The simulated stream–aquifer exchanges should be negative all along the Rhine River. In this study, this is the case for all the simulations in Fig. 10 except the PSRTM simulation. Moreover, the corrected topography allows one to improve the strong positive biases of piezometric heads simulated with PSRTM and located over the southeastern part of the aquifer. These improvements are only due to a lower river level defined

for PHY on the first tributary of the Rhine shown in green in Fig. 13 and illustrate the importance of choosing a well-defined river water level in regional hydrogeological modeling.

The fluctuations of the river levels affect the simulation of the piezometric heads. Whatever the method used (rating curves or Manning's formula), the comparison between observed and simulated piezometric heads is improved with respect to the simulations with fixed river levels (Fig. 5) and shows the relevance of the geomorphological relationships based on observations that are proposed in this study to determine the elevation of the riverbed (Eq. 8). Nevertheless, the Manning formula seems to give better results than the rating curves. Indeed, the correlations computed for the piezometric heads and the river levels are better with VMAN than with VRC; moreover, the fluctuating river levels of VMAN have a more pronounced effect on the piezometric heads than VRC (Fig. 7). These differences are mostly due to the fact that the rating curves cannot be defined for all the river cells because of the lack of observations for some rivers or tributaries (see Fig. 2). Conversely, the computation of the fluctuating river levels is possible on all the cells with the Manning formula; however, the Manning formula seems to overestimate the simulation of the river water levels, in particular for the Rhine River (see Fig. 10). Such behavior can be attributed to the uncertainties remaining on the hypothesis for defining the cross section of the river and the geomorphological parameters (width, elevation of the riverbed, slope and Manning's coefficient). Moreover, the Rhine River is strongly anthropized and the river discharge is influenced by the numerous dams, thresholds, and human withdrawals—for example for supplying the needs of nuclear plants.

The fluctuating river water levels also affect the simulation of the surface-water/groundwater interactions. The recharge from the river to the aquifer is slightly increased (see Table 1). Moreover, the agreement between the observed wetlands and the simulated groundwater overflows appear to be better. These elements confirm the relevance of the corrections applied to the topography as well as the new geomorphological relationship describing the elevation of the riverbed. This study also points out the need for data to better estimate the river levels at regional scale, both for parameterizing the models and evaluating the simulated hydrological variables. Such need could be fulfilled by the future Surface Water and Ocean Topography satellite mission, which will provide estimations of land surface water with a spatial resolution of about 50–100 m (Häfliger et al. 2015; Biancamaria et al. 2016).

**Funding Information** This study was partly funded by the Office National de l'Eau et des Milieux Aquatiques (ONEMA) within the framework of the Naprom and by the TOSCA CNES project "Intérêt des données SWOT pour l'hydrologie et l'hydrodynamique à l'échelle régionale" convention CNES No. 92532.

**Open Access** This article is distributed under the terms of the Creative Commons Attribution 4.0 International License (<http://creativecommons.org/licenses/by/4.0/>), which permits unrestricted use, distribution, and reproduction in any medium, provided you give appropriate credit to the original author(s) and the source, provide a link to the Creative Commons license, and indicate if changes were made.

## References

- Arora VK, Boer GJ (1999) A variable velocity flow routing algorithm for GCMs. *J Geophys Res* 104(D24):30965–30979. <https://doi.org/10.1029/1999JD900905>
- Barthel R, Banzhaf S (2016) Groundwater and surface water interaction at the regional-scale: a review with focus on regional integrated models. *Water Resour Manag* 30:1–32. <https://doi.org/10.1007/s11269-015-1163-z>
- Biancamaria S, Lettenmaier DP, Pavelsky TM (2016) The SWOT mission and its capabilities for land hydrology. *Surv Geophys* 37:307–337. <https://doi.org/10.1007/s10712-015-9346-y>
- Boukerma B (1987) Modélisation des écoulements superficiels et souterrains dans le sud-ouest de la France: approche du bilan hydrique [Modeling of superficial and groundwater flows in southwestern France: a water balance approach]. Ecole Nationale Supérieure des Mines de Paris, Paris
- Brasington J, Vericat D, Rychkov I (2012) Modeling river bed morphology, roughness, and surface sedimentology using high resolution terrestrial laser scanning. *Water Resour Res* 48:W11519. <https://doi.org/10.1029/2012WR012223>
- Chandesris A, Mengin N, Maiavoi JR, Souchon Y, Wasson JG (2009) SYstème Relationnel d'Audit de l'Hydromorphologie des Cours d'Eau SYRAH-CE [Relation system for the hydromorphology of watercourses SYRH-EC]. Large scale atlas V2.0, IRSTEA Eaux, Barres, France
- Dai X, Wan R, Yang G (2015) Non-stationary water-level fluctuation in China's Poyang Lake and its interactions with Yangtze River. *J Geogr Sci* 25:274–288. <https://doi.org/10.1007/s11442-015-1167-x>
- David CH, Habets F, Maidment DR, Yang Z-L (2011) RAPID applied to the SIM-France model. *Hydrol Process* 25:3412–3425. <https://doi.org/10.1002/hyp.8070>
- Decharme B, Douville H, Prigent C, Papa F, Aires F (2008) A new river flooding scheme for global climate applications: off-line evaluation over South America. *J Geophys Res* 113:11. <https://doi.org/10.1029/2007JD009376>
- Doble R, Brunner P, McCallum J, Cook PG (2012) An analysis of river bank slope and unsaturated flow effects on bank storage. *Ground Water* 50:77–86. <https://doi.org/10.1111/j.1745-6584.2011.00821.x>
- Doble R, Crosbie R, Peeters L, Joehnk K, Ticehurst C (2014) Modelling overbank flood recharge at a continental scale. *Hydrol Earth Syst Sci* 18:1273–1288. <https://doi.org/10.5194/hess-18-1273-2014>
- Döll P, Douville H, Güntner A, Schmied HM, Wada Y (2016) Modelling freshwater resources at the global scale: challenges and prospects. *Surv Geophys* 37:195–221. <https://doi.org/10.1007/s10712-015-9343-1>
- Fan Y (2015) Groundwater in the Earth's critical zone: relevance to large-scale patterns and processes. *Water Resour Res* 51:3052–3069. <https://doi.org/10.1002/2015WR017037>
- Fan Y, Miguez-Macho G, Weaver CP, Walko R, Robock A (2007) Incorporating water table dynamics in climate modeling: 1. water table observations and equilibrium water table simulations. *J Geophys Res* 112:D10125. <https://doi.org/10.1029/2006JD008111>
- Farr TG, Rosen PA, Caro E, Crippen R, Duren R, Hensley S, Kobrick M, Paller M, Rodriguez E, Roth L, Seal D, Shaffer S, Shimada J,

- Umland J, Werner M, Oskin M, Burbank D, Alsdorf D (2007) The shuttle radar topography mission. *Rev Geophys* 45:RG2004. <https://doi.org/10.1029/2005RG000183>
- Flipo N, Mouhri A, Labarthe B, Biancamaria S (2014) Continental hydrosystem modelling: the concept of nested stream–aquifer interfaces. *Hydrol Earth Syst Sci Discuss* 11:451–500. <https://doi.org/10.5194/hessd-11-451-2014>
- Gomez E (2002) Modélisation intégrée du transfert de nitrate à l'échelle régionale dans un système hydrologique: application au bassin de la Seine [Integrated modeling of nitrogen transport at the regional scale in a hydrologic system: application in the Seine basin]. École Nationale Supérieure des Mines de Paris, Paris
- Graham DN, Butts MB (2005) Flexible, integrated watershed modelling with MIKE SHE. In: *Watershed models*. CRC, Boca Raton, FL, pp 245–272
- Habets F, Etchevers P, Golaz C, Leblois E, Ledoux E, Martin E, Noilhan J, Otlé C (1999) Simulation of the water budget and the river flows of the Rhone basin. *J Geophys Res* 104:31145–31,172. <https://doi.org/10.1029/1999JD901008>
- Habets F, Gascoïn S, Korkmaz S, Thiéry D, Zribi M, Amraoui N, Carli M, Ducharne A, Leblois E, Ledoux E, Martin E, Noilhan J, Otlé C, Viennot P (2010) Multi-model comparison of a major flood in the groundwater-fed basin of the Somme River (France). *Hydrol Earth Syst Sci* 14:99–117. <https://doi.org/10.5194/hess-14-99-2010>
- Häfliger V, Martin E, Boone A, Habets F, David CH, Garambois P-A, Roux H, Ricci S, Berthon L, Thévenin A, Biancamaria S (2015) Evaluation of regional-scale river depth simulations using various routing schemes within a hydrometeorological modeling framework for the preparation of the SWOT mission. *J Hydrometeorol* 16:1821–1842. <https://doi.org/10.1175/JHM-D-14-0107.1>
- Heritage GL, Milan DJ, Large ARG, Fuller IC (2009) Influence of survey strategy and interpolation model on DEM quality. *Geomorphology* 112:334–344. <https://doi.org/10.1016/j.geomorph.2009.06.024>
- Javemick L, Brasington J, Caruso B (2014) Modeling the topography of shallow braided rivers using structure-from-motion photogrammetry. *Geomorphology* 213:166–182. <https://doi.org/10.1016/j.geomorph.2014.01.006>
- Käser D, Graf T, Cochand F, McLaren R, Therrien R, Brunner P (2014) Channel representation in physically based models coupling groundwater and surface water: pitfalls and how to avoid them. *Ground Water* 52:827–836. <https://doi.org/10.1111/gwat.12143>
- Kellndorfer J, Walker W, Pierce L, Dobson C, Fites JA, Hunsaker C, Vona J, Clutter M (2004) Vegetation height estimation from Shuttle Radar Topography Mission and national elevation datasets. *Remote Sens Environ* 93:339–358. <https://doi.org/10.1016/j.rse.2004.07.017>
- Kollet SJ, Maxwell RM (2006) Integrated surface–groundwater flow modeling: a free-surface overland flow boundary condition in a parallel groundwater flow model. *Adv Water Resour* 29:945–958. <https://doi.org/10.1016/j.advwatres.2005.08.006>
- Koster RD, Suarez MJ (2001) Soil moisture memory in climate models. *J Hydrometeorol* 2:558–570. [https://doi.org/10.1175/1525-7541\(2001\)002<0558:SMMICM>2.0.CO;2](https://doi.org/10.1175/1525-7541(2001)002<0558:SMMICM>2.0.CO;2)
- Lange J (2005) Dynamics of transmission losses in a large arid stream channel. *J Hydrol* 306:112–126. <https://doi.org/10.1016/j.jhydrol.2004.09.016>
- Ledoux E, Girard G, Villeneuve JP (1984) Proposition d'un modèle couplé pour la simulation conjointe des écoulements de surface et des écoulements souterrains sur un bassin hydrologique [Suggestion for a coupled model of surface and groundwater simulation on a watershed]. *Houille Blanche* 1–2:101–120. <https://doi.org/10.1051/lhb/1984005>
- Ledoux E, Girard G, De Marsily G (1989) Spatially distributed modeling: conceptual approach, coupling surface water and groundwater. In: *Unsaturated flow in hydrologic modeling: theory and practice*. Kluwer, Dordrecht, The Netherlands, pp 435–454
- LUBW (2006) INTERREG III A: MoNit “Modélisation de la pollution des eaux souterraines par les nitrates dans la vallée du Rhin Supérieur” [Modeling groundwater nitrate pollution in the Upper Rhine Valley]. Technical report LUBW, LBUW, Karlsruhe, Germany
- Mahfouf J-F, Manzi AO, Noilhan J, Giordani H, DéQué M (1995) The land surface scheme ISBA within the Météo-France climate model ARPEGE: part I, implementation and preliminary results. *J Clim* 8:2039–2057. [https://doi.org/10.1175/1520-0442\(1995\)008<2039:TLSSIW>2.0.CO;2](https://doi.org/10.1175/1520-0442(1995)008<2039:TLSSIW>2.0.CO;2)
- Majdalani S, Ackerer P (2011) Identification of groundwater parameters using an adaptative multiscale method. *Ground Water* 49:548–559. <https://doi.org/10.1111/j.1745-6584.2010.00750.x>
- Masson V, Le Moigne P, Martin E, Faroux S, Alias A, Alkama R, Belamari S, Barbu A, Boone A, Bouyssel F, Brousseau P, Brun E, Calvet J-C, Carrer D, Decharme B, Delire C, Donier S, Essaouini K, Gibelin A-L, Giordani H, Habets F, Jidane M, Kerdraon G, Kourzeneva E, Lafaysse M, Lafont S, Lebeauin Brossier C, Lemonsu A, Mahfouf J-F, Marguinaud P, Mokhtari M, Morin S, Pigeon G, Salgado R, Seity Y, Taillefer F, Tanguy G, Tulet P, Vincendon B, Vionnet V, Voldoire A (2013) The SURFEXv7.2 land and ocean surface platform for coupled or offline simulation of earth surface variables and fluxes. *Geosci Model Dev* 6:929–960. <https://doi.org/10.5194/gmd-6-929-2013>
- Ministère de l'Écologie, du Développement Durable et de l'Énergie (2015) Banque HYDRO (HYDRO Database). <http://hydro.eaufrance.fr/>. Accessed 9 April 2018
- Monteil C, Flipo N, Poulin M, Habets F, Krimissa M, Ledoux E (2010) Assessing the contribution of the main aquifer units of the Loire basin to river discharge during low flow. XVIII International Conference on Water Resources, Barcelona, June 2010
- Noilhan J, Donier S, Lacarrère P, Sarrat C, Moigne PL (2011) Regional-scale evaluation of a land surface scheme from atmospheric boundary layer observations. *J Geophys Res* 116:D011104. <https://doi.org/10.1029/2010JD014671>
- Orlandini S, Rosso R (1998) Parameterization of stream channel geometry in the distributed modeling of catchment dynamics. *Water Resour Res* 34:1971–1985. <https://doi.org/10.1029/98WR00257>
- Paiva RCD, Collischonn W, Tucci CEM (2011) Large scale hydrologic and hydrodynamic modeling using limited data and a GIS based approach. *J Hydrol* 406:170–181. <https://doi.org/10.1016/j.jhydrol.2011.06.007>
- Rabus B, Eineder M, Roth A, Bamler R (2003) The Shuttle Radar Topography Mission: a new class of digital elevation models acquired by spaceborne radar. *ISPRS J Photogramm Remote Sens* 57:241–262. [https://doi.org/10.1016/S0924-2716\(02\)00124-7](https://doi.org/10.1016/S0924-2716(02)00124-7)
- Rupp DE, Larned ST, Arscott DB, Schmidt J (2008) Reconstruction of a daily flow record along a hydrologically complex alluvial river. *J Hydrol* 359:88–104. <https://doi.org/10.1016/j.jhydrol.2008.06.019>
- Rushton K (2007) Representation in regional models of saturated river–aquifer interaction for gaining/losing rivers. *J Hydrol* 334:262–281. <https://doi.org/10.1016/j.jhydrol.2006.10.008>
- Saleh F, Flipo N, Habets F, Ducharme A, Oudin L, Viennot P, Ledoux E (2011) Modeling the impact of in-stream water level fluctuations on stream–aquifer interactions at the regional scale. *J Hydrol* 400:490–500. <https://doi.org/10.1016/j.jhydrol.2011.02.001>
- Saleh F, Ducharme A, Flipo N, Oudin L, Ledoux E (2013) Impact of river bed morphology on discharge and water levels simulated by a 1D Saint-Venant hydraulic model at regional scale. *J Hydrol* 476:169–177. <https://doi.org/10.1016/j.jhydrol.2012.10.027>
- Sanford W (2002) Recharge and groundwater models: an overview. *Hydrogeol J* 10:110–120. <https://doi.org/10.1007/s10040-001-0173-5>
- Schäppi B, Perona P, Schneider P, Burlando P (2010) Integrating river cross section measurements with digital terrain models for improved

- flow modelling applications. *Comput Geosci* 36:707–716. <https://doi.org/10.1016/j.cageo.2009.12.004>
- Schumann G, Matgen P, Cutler MEJ, Black A, Hoffmann L, Pfister L (2008) Comparison of remotely sensed water stages from LiDAR, topographic contours and SRTM. *ISPRS J Photogramm Remote Sens* 63:283–296. <https://doi.org/10.1016/j.isprsjprs.2007.09.004>
- Sophocleous M (2002) Interactions between groundwater and surface water: the state of the science. *Hydrogeol J* 10:52–67. <https://doi.org/10.1007/s10040-001-0170-8>
- Sun G, Ranson KJ, Kharuk VI, Kovacs K (2003) Validation of surface height from Shuttle Radar Topography Mission using shuttle laser altimeter. *Remote Sens Environ* 88:401–411. <https://doi.org/10.1016/j.rse.2003.09.001>
- Sun X, Bernard-Jannin L, Gameau C, Volk M, Arnold JG, Srinivasan R, Sauvage S, Sanchez-Pérez J-M (2016) Improved simulation of river water and groundwater exchange in an alluvial plain using the SWAT model. *Hydrol Process* 30:187–202. <https://doi.org/10.1002/hyp.10575>
- The Ramsar Convention Secretariat (2014) Ramsar Sites Information Service. <https://rsis Ramsar.org/>. Accessed 9 April 2018
- Thierion C, Longuevergne L, Habets F, Ledoux E, Ackerer P, Majdalani S, Leblois E, Lecluse S, Martin E, Queguiner S, Viennot P (2012) Assessing the water balance of the Upper Rhine Graben hydrosystem. *J Hydrol* 424–425:68–83. <https://doi.org/10.1016/j.jhydrol.2011.12.028>
- Thiéry D (2015) Code de calcul MARTHE: modélisation 3D des écoulements dans les hydrosystèmes—notice d'utilisation de la version 7.5 [MARTHE: modeling software for groundwater flows—manual for version 7.5]. BRGM/RP-64554-FR, BRGM, Orléans, France
- Thompson JR, Sorenson HR, Gavin H, Refsgaard A (2004) Application of the coupled MIKE SHE/MIKE 11 modelling system to a lowland wet grassland in southeast England. *J Hydrol* 293:151–179. <https://doi.org/10.1016/j.jhydrol.2004.01.017>
- Trémolières M, Eglin I, Roeck U, Carbiener R (1993) The exchange process between river and groundwater on the Central Alsace floodplain (eastern France). *Hydrobiologia* 254:133–148. <https://doi.org/10.1007/BF00014108>
- Vergnes J-P, Decharme B, Habets F (2014) Introduction of groundwater capillary rises using subgrid spatial variability of topography into the ISBA land surface model. *J Geophys Res Atmos* 119(19):11065–11086. <https://doi.org/10.1002/2014JD021573>
- Winter TC (1999) Relation of streams, lakes, and wetlands to groundwater flow systems. *Hydrogeol J* 7:28–45. <https://doi.org/10.1007/s100400050178>
- Woessner WW (2000) Stream and fluvial plain ground water interactions: rescaling hydrogeologic thought. *Ground Water* 38:423–429. <https://doi.org/10.1111/j.1745-6584.2000.tb00228.x>
- Yeh PJ-F, Eltahir EAB (2005) Representation of water table dynamics in a land surface scheme, part II: subgrid variability. *J Clim* 18:1881–1901. <https://doi.org/10.1175/JCLI3331.1>
- Zhang J, Ross M (2015) Comparison of IHM and MIKE SHE model performance for modeling hydrologic dynamics in shallow water table settings. *Vadose Zone J* 14:7. <https://doi.org/10.2136/vzj2014.03.0023>